On the Stability of the Passive Dynamics of Quadrupedal Running with a Bounding Gait

Ioannis Poulakakis
Control Systems Laboratory
Department of Electrical Engineering
and Computer Science
The University of Michigan
Ann Arbor, MI 48109, USA
poulakas@eecs.umich.edu

Evangelos Papadopoulos
Department of Mechanical Engineering
National Technical University of Athens
Athens, 15780, Greece
egpapado@central.ntua.gr

Martin Buehler
Boston Dynamics
Cambridge, MA 02139, USA
buehler@BostonDynamics.com

Abstract

This paper examines the passive dynamics of quadrupedal bounding. First, an unexpected difference between local and global behavior of the forward speed versus touchdown angle in the self-stabilized Spring Loaded Inverted Pendulum (SLIP) model is exposed and discussed. Next, the stability properties of a simplified sagittal plane model of our Scout II quadrupedal robot are investigated. Despite its simplicity, this model captures the targeted steady state behavior of Scout II without dependence on the fine details of the robot structure. Two variations of the bounding gait, which are observed experimentally in Scout II, are considered. Surprisingly, numerical return map studies reveal that passive generation of a large variety of cyclic bounding motion is possible. Most strikingly, local stability analysis shows that the dynamics of the open loop passive system alone can confer stability to the motion! These results can be used in developing a general control methodology for legged robots, resulting from the synthesis of feedforward and feedback models that take advantage of the mechanical system, and might explain the success of simple, open loop bounding controllers on our experimental robot.

KEY WORDS—passive dynamics, bounding gait, dynamic running, quadrupedal robot

1. Introduction

Mobility and versatility are the most important reasons for building legged robots, instead of wheeled and tracked ones, and for studying legged locomotion. Animals exhibit impressive performance in handling rough terrain, and they can reach a much larger fraction of the earth landmass on foot than existing wheeled vehicles. Most mobile robotic applications can benefit from the improved mobility and versatility that legs offer.

Early attempts to design legged platforms resulted in slow moving, statically stable robots; these robot designs are still the most prevalent today, see Berns (2006) for a survey. In this paper, however, we restrict our attention to dynamically stable legged robots. Twenty years ago Raibert (1986) set the stage with his groundbreaking work on dynamic legged robots by introducing a three-part controller for stabilizing running on his one-, two-, and four-legged machines. His controllers, although very simple, resulted in high performance, robust running with different gaits, such as the trot, the pace, and the bound. Inspired by Raibert's work, Buehler and his collaborators at McGill's Ambulatory Robotics Laboratory (ARL)

Portions of this paper have previously appeared in conference publications Poulakakis, Papadopoulos, and Buehler (2003) and Poulakakis, Smith, and Buehler (2005b). The first and third authors were with the Centre for Intelligent Machines at McGill University when this work was performed. Address all correspondence related to this paper to the first author.

The International Journal of Robotics Research
Vol. 25, No. 7, July 2006, pp. 669-687
DOI: 10.1177/0278364906066768

Figures appear in color online: http://ijr.sagepub.com

designed and built power autonomous one-, four-, and six-legged platforms, which demonstrate walking and running in a dynamic fashion; see Buehler (2002) for an overview. Minimal actuation, coupled with a suitably designed mechanical system featuring compliant legs, and simple control laws that excite the natural dynamics of the mechatronic system are the fundamental principles exemplified by ARL's robots.

Other design and control approaches for dynamically stable running robots have been proposed, including the Patrush and Tekken robotic quadrupeds by Kimura and his collaborators (Kimura, Akiyama, and Sakurama 1998; Fukuoka, Kimura, and Cohen 2003). Based on principles from neurobiology, they implemented bounding by transitioning from pronking in Patrush by combining compliant legs with a neural oscillator network (Kimura, Akiyama, and Sakurama 1998). More recently, Fukuoka, Kimura, and Cohen (2003) proposed a controller based on a Central Pattern Generator (CPG) that alters its active phase based on sensory feedback and results in adaptive dynamic walking on irregular terrain. Following a different design approach, Cham et al. (2002) introduced Sprawlita, a spectacularly robust dynamic hexapod, capable of running with speeds over four body lengths per second on irregular terrains with hip height obstacles. The authors employed a novel manufacturing technique to construct a biomimetic mechanism with actuators, sensors and wiring embedded in the robot's body and limbs.

Despite their morphological and design differences these robots walk and run using control laws without intense feedback. For instance, recent research on our quadrupedal robot Scout II (Figure 1) demonstrated that simple controllers, requiring only touchdown detection and local feedback from motor encoders, can be used to stabilize running, (Poulakakis, Smith, and Buehler 2005a, 2005b). These controllers simply position the legs at a fixed touchdown angle during the flight phase, and result in stable bounding with speeds up to 1.3 m/s. A slightly modified control strategy was successfully implemented on Scout II to result in the first ever reported robot gallop gait (Smith and Poulakakis 2004; Poulakakis, Smith, and Buehler 2005b). Similar design and control ideas as found in Scout II have subsequently been implemented to generate bounding in a modified (one actuator per leg) version of the SONY AIBO dog (Yamamoto et al. 2001), and in the one-actuator-per-leg hexapedal RHex, (Campbell and Buehler 2003; see Saranli, Buehler, and Koditschek 2001 for design and control details). Recently RHex traversed irregular terrain with speeds over five body lengths per second and reduced specific resistance (Weingarten et al. 2004). Once again the controller employs only local feedback from encoders, necessary for the leg recirculation strategy, while the parameters for some of its gaits are determined via Nelder-Mead optimization (Weingarten et al. 2004).

On the other hand, Stanford's Sprawlita runs without any sensory feedback at all (Cham et al. 2002). Leg placement in the sagittal plane is achieved via a passive compliant hip joint, acting in a manner analogous to that of the trochanter–femur joint of a cockroach, while the legs are equipped with prismatic actuators (pneumatic pistons) and behave mainly as thrusters (Cham et al. 2002). Furthermore, an extreme case, where no control action is needed, was first presented by McGeer (1990) in his pioneering work on passive walking. McGeer built a gravity-powered biped, which was able to walk on inclined surfaces without the need of sensors and actuators. He also expanded his analysis to passive bipedal running in McGeer (1989), without, though, providing experimental results.

Fig. 1. Scout II: a high performance, power autonomous, four-legged robot with one actuator per leg.

In a loose sense, the experimental findings in robotics are in qualitative agreement with developments in biology. For instance, experimental evidence suggests that the high level nervous system is not required for steady state level walking and running, and that mechanisms entirely located within the spinal cord are responsible for generating the rhythmic motions of the legs during locomotion (Pearson 1976; McMahon 1985). Furthermore, locomotion is possible even when feedback from the afferent pathways is denied[1] (de-afferented spinal walking; McMahon 1985). On the other hand, recent research in physiology indicates that, during rapid locomotion, the control is dominated by the mechanical system (Full and Koditschek 1999; Kubow and Full 1999). To explore the role of the mechanical system in control, Kubow and Full (1999) developed a simple, two-dimensional, dynamic model of a hexapedal runner (death-head cockroach, *Blaberous discoidalis*). The model had no equivalent of nervous feedback among any of its components and it was found to be inherently stable. This work first revealed the significance of *mechanical* feedback in simplifying neural control, by demonstrating that stability could result from leg moment arm changes alone.

1. However, when the afferent nerves are intact, sensory input reinforces and modulates the centrally generated pattern (McMahon 1985).

Therefore, one can assume that intense control action relying on complex feedback from a multitude of sensory receptors is not necessary to generate and sustain walking and running.

In an attempt to set the basis for a systematic approach in studying legged locomotion Full and Koditschek (1999) introduced the *templates* and *anchors* modeling and control hierarchy. Schmitt and Holmes (2002) proposed the *Lateral Leg Spring (LLS)* template to analyze the horizontal dynamics of sprawl-postured animals. Surprisingly they found that, despite its conservative nature, the LLS template exhibits some degree of asymptotic stability without the need of feedback control laws. To study the basic properties of sagittal plane running, the *Spring Loaded Inverted Pendulum (SLIP)* template has been proposed (see Schwind 1998 and references therein) which, despite its structural simplicity, was found to sufficiently encode the task-level behavior of animals and robots (Full and Koditschek 1999). Recent research conducted independently by Seyfarth et al. (2002), and Ghigliazza et al. (2003), showed that when the SLIP is supplied with the appropriate initial conditions, and for certain touchdown angles, not only does it follow a cyclic motion, but it also tolerates small perturbations without the need of a feedback control law. The inherent stability of SLIP and LLS models is a very interesting property since, as is known from mechanics, systems described by autonomous, conservative, holonomically constrained flows cannot be asymptotically stable.[2] However, Altendorfer, Koditschek and Holmes (2004) showed that the stable behavior of piecewise holonomic conservative systems is a consequence of their hybrid nature.

The formal connection between templates, such as the SLIP, and more elaborate models, which enjoy a more faithful correspondence to the morphology of the robot, has not yet been fully investigated; for preliminary results, see Saranli and Koditschek (2003). Furthermore, as was shown in Cherouvim and Papadopoulos (2005), controllers specifically derived for the SLIP will have to be modified in order to be successful in inducing stable running in more complete models that include pitch dynamics and comprise energy losses. However, simplified models have been proved to be helpful in the design of controllers that exploit the passive dynamics of the system, resulting in considerable energy savings, which is a critical requirement for autonomous legged locomotion. A notable example of such controllers is ARL's Monopod II, see Ahmadi and Buehler (1997, 1999). Monopod II exploits the passive dynamics through the use of leg and hip compliance to keep energy expenditure for maintaining the vertical and hip oscillations at a minimum. Proper initial conditions and selection of compliant elements, together with a controller that synchronizes the vertical and hip oscillations, result in motions close to passive dynamic operation with a dramatic decrease in energy requirements; 70% reduction in specific resistance was measured in experiments (Ahmadi and Buehler 1999).

Other models have also been proposed to study sagittal running of dynamically stable quadrupeds. Murphy and Raibert studied pronking and bounding using a model with kneed legs, whose lengths were controllable (Murphy 1985). They discovered that active attitude control in bounding is not necessary when the body's moment of inertia is smaller than the mass times the square of half the hip spacing (see also Raibert 1986, p. 193). Following that work, Berkemeier (1998) showed that Murphy's result applies to a simple, linearized, running-in-place model, and that it can be extended to pronking under appropriate conditions. These models (Murphy 1985; Berkemeier, 1998) are both actuated and comprise energy losses. To the best of the authors' knowledge, only Brown (1985) investigated the conditions for obtaining passive cyclic motion. He studied two limiting cases of system behavior: the grounded and the flight regimes, and found that the system in either regime can passively trot, gallop or bound under the appropriate initial conditions, *only*[3] when its properties—mass m, moment of inertia I, and half hip spacing L—have the particular relationship $I/mL^2 = 1$.

In this paper, motivated by the experimental findings in our robot and in others, we attempt to provide an explanation for simple control laws being adequate in stabilizing complex running tasks such as bounding. It is the simplicity of Scout II's design and control together with its experimental success that initiated our attempts for this study. Our analysis departs from the recent developments regarding the self-stabilization property of the SLIP briefly described in Section 3, where it is shown that self-stabilization cannot be immediately applied to improve the existing intuitive control algorithms. To investigate passive stability in Scout II, a simple mechanical model that encodes the targeted task-level behavior (steady state bounding) is proposed in Section 4. The model is unactuated and conservative, so that the properties of the natural dynamics of Scout II can be revealed. In that respect, it represents an extension of the SLIP suitable for studying bounding, in which pitching is a very important component of the motion that is not captured by point-mass models like the SLIP.

Identifying conditions that permit the generation of passive running cycles and studying their stability properties constitutes the central contribution of this paper. To do so, a Poincaré return map, whose fixed points describe the cyclic bounding motion, is derived and studied numerically. Two variations of the bounding gait, which are of experimental interest in Scout II, are analyzed. It is found that both can be passively generated as a response of the system to an appropriate set of initial conditions. Most strikingly, a regime where the system is self-stabilized against small perturbations from the nominal conditions is identified. These results show that bounding is

2. By Liouville's theorem (see Scheck 1999, p. 122), the incompressibility of the phase fluid precludes the existence of asymptotically stable equilibria in Hamiltonian systems, for if such points existed, they would reduce a finite volume in the phase space to a single point.

3. However, in Sections 5 and 6 it will be shown that a conservative model of Scout II can passively pronk and bound despite the fact that its parameters satisfy the inequality $I/mL^2 < 1$.

essentially a natural mode of the system, and that only minor control action and energy are required keep the robot running.

It must be emphasized that the practical motivation for studying the *passive dynamics* is threefold. First, if the system remains close to its passive behavior, then the actuators have less work to do to maintain the motion, and energy efficiency, a very important issue in mobile robots, is improved (an example of how this principle is applied conceptually and in experiments is provided by the ARL Monopod II; Ahmadi and Buehler 1997,1999). Second, if there are operating regimes where the system is passively stable, then active stabilization is either not required, or else will require less control effort and sensing. Finally, passive dynamics can be used as a design tool to specify the desirable behavior of complex, underactuated dynamical systems, where reference trajectory tracking is not possible. It is important to note that the purpose of this paper is not to propose a model of Scout II that achieves a faithful correspondence to the robot's structure and function, and is suitable for constructing accurate simulations that reproduce exactly the data collected in experiments. Such a model was presented in detail in Poulakakis, Smith, and Buehler (2005a). Rather, in this paper a simplified model is analyzed, which encodes the targeted behavior and reveals the basic properties of quadrupedal bounding, without dependence on the fine details of the robot structure.

It is worth mentioning that, since our original work on the stability analysis of the passive dynamics of quadrupedal bounding, first reported in Poulakakis (2002), Poulakakis, Papadopoulos, and Buehler (2003) and Poulakakis, Smith, and Buehler (2005b), other researchers, for example Iida and Pfeifer (2004) and Zhang, Fukuoka, and Kimura (2004), have adopted similar approaches to study running, revealing similar aspects of the passive dynamics of their robotic quadrupeds, and confirming our early results, which are anticipated to facilitate the design of legged locomotion controllers that take advantage of the system's natural dynamics.

2. Experiments with Scout II: the Bounding Gait

Scout II has been designed for power autonomous operation; the hip assemblies contain the actuators and batteries, and the body houses all computing, interfacing and power distribution. The most significant feature of Scout II is the fact that it uses a *single* actuator per leg located at the hip joint. Each leg assembly consists of a lower and an upper leg, connected via a spring to form a compliant prismatic joint. Thus, each leg has two degrees of freedom (DOF): the hip DOF (actuated), and the linear compliant DOF (passive); for details regarding the design of Scout II see Poulakakis, Smith, and Buehler (2005a) and references therein.

In bounding, Scout II uses its front and back legs in pairs, thus the essentials of the motion take place in the sagittal plane. According to the virtual leg concept (Raibert 1986), the back and front physical leg pairs can be replaced by single back and front virtual legs, respectively. Each of the back and front virtual legs detects three leg states: "flight", "stance-retraction" and "stance-brake", which are separated by touchdown, sweep limit, and liftoff events respectively, see Figure 2. During the "flight" state, the controller places the leg to a desired, *fixed* throughout the gait, touchdown angle. Then, during the "stance-retraction" state, the leg is swept back by applying a torque according to the saturation limitations of the motor, until the sweep limit is reached. In the "stance-brake" state the leg is kept at the sweep limit angle. There is no actively controlled coupling between the back and front virtual legs – the bounding motion is purely the result of the controller interaction through the multi-body dynamic system. Furthermore, it must be emphasized that state changes are made based on data from only two types of sensors: the legs' linear potentiometers, which are used to detect touchdown and liftoff, and the legs' motor encoders, which allow state transition when the pre-specified sweep limit angle is reached.

This controller, documented in detail in Poulakakis, Smith, and Buehler (2005a), results in the bounding gait presented in Figure 3, where two variations in the footfall pattern can be observed. In the first variation, which is referred to as *bounding with double stance*, the front leg touchdown occurs directly after the back leg touchdown event, thus there is a portion of the cycle where both the front and back legs are in stance (double leg stance phase), see Figure 3. On the other hand, in the second bounding variation, which is referred to as *bounding without double stance*, the front leg touchdown occurs after the back leg liftoff event, thus the back and front leg stance phases are separated by a double flight phase, as the dashed line shows in Figure 3. In experiments, the robot converges to either of the two variations depending on the system's energy content at steady state; for instance, at higher speeds and pitch rates the robot shows preference for the bounding without double stance.

Scout II is a nonlinear, highly underactuated, system that exhibits intermittent dynamics. The complexity is further increased by the limited ability in applying hip torques due to actuator and friction constraints, and by the existence of unilateral ground forces. On the other hand, running is generally considered a complex task involving the coordination of many limbs and redundant degrees of freedom, and in general, it cannot be encoded in a set of outputs following prespecified desired trajectories, imposed on the system using the actuator inputs.[4]

Despite this complexity, simple control laws requiring minimal sensing, such as the one presented in Figure 2, were

4. It must be pointed out that, for certain legged systems exhibiting one degree of underactuation, it is possible to define a set of outputs whose tracking guarantees the successful accomplishment of the task (Grizzle, Abba, and Plestan 2001). However, Scout II not only exhibits two degrees of underactuation during the stance phases, but also certain outputs are related to the inputs via coupling terms that become singular during the motion, thus significantly reducing control affordance.

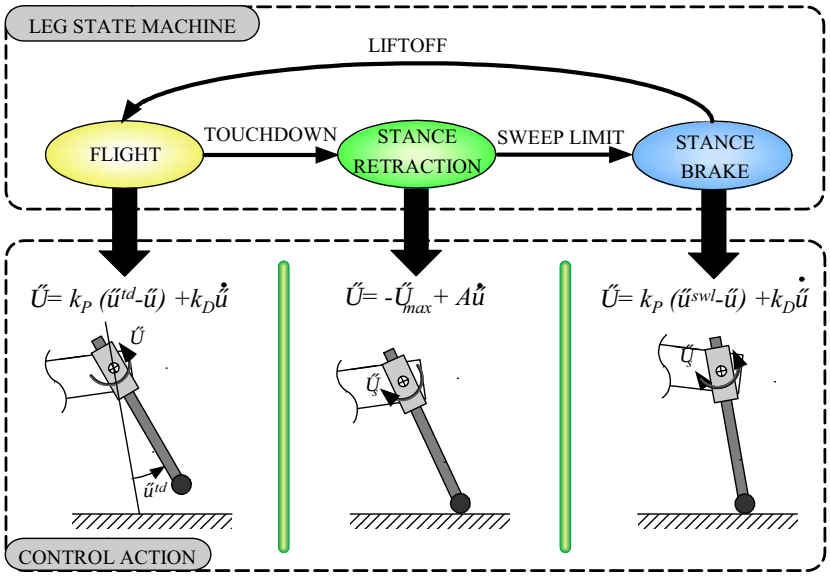

Fig. 2. The virtual leg state machine and corresponding commanded torques (τ_{max} and A are the offset and the slope of the motor's torque speed line; for details see Poulakakis, Smith, and Buehler (2005a), where the gains and set points are also presented).

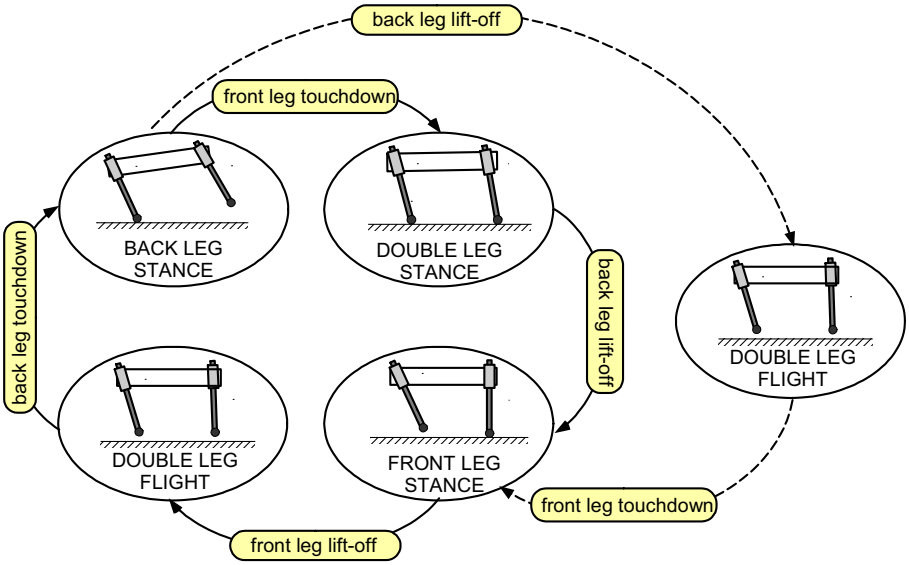

Fig. 3. Bounding phases and events with and without double leg stance.

found to excite and stabilize periodic motions, resulting in robust and fast running. Indeed, the controller described above does *not* require any task-level feedback such as forward velocity. The absence of forward velocity feedback in adjusting the back and front leg touchdown angles, which are kept constant throughout the motion, constitutes a significant difference between the controller described here and in Poulakakis, Smith, and Buehler (2005a), and Raibert's (1986) bounding controller. Interestingly, as will be described in Section 3, Raibert's velocity controller cannot predict the fact that stable cyclic motion can be achieved in the SLIP template by keeping the touchdown angle constant throughout the motion.

In fact, Scout II's controller, not only does not require any task-level feedback, but it also does *not* require any body state feedback: one only needs to know the position of the leg with respect to the body and its state (flight, stance-retraction and stance-brake). It is therefore natural to ask why such a complex system can accomplish such a complex task via minor control action. As outlined in this paper, a possible answer is that Scout II's unactuated, conservative dynamics *already* exhibits stable bounding cycles, and hence a simple controller is all that is needed for keeping the robot bounding.

3. Self-stabilization in the SLIP: a Starting Point

The purpose of this section is to motivate the analysis of the stability of the passive dynamics of quadrupedal bounding through a brief description of the self-stabilization property recently discovered in the SLIP. Rather than analyzing the much studied SLIP (Schwind 1998; Full and Koditschek 1999; Cham, Bailey, and Cutkosky 2000; Seyfarth et al. 2002; Ghigliazza et al. 2003; Altendorfer, Koditschek, and Holmes 2004; Cherouvim and Papadopoulos 2005), we turn our attention to its implications for the control of legged robots. We demonstrate that the mechanism that results in self-stabilization is not yet fully understood, at least in a way that would immediately be applicable to improve the existing intuitive control algorithms.

The SLIP, see Figure 4, consists of a point mass atop a spring and it is passive (no torque inputs) and conservative (no energy losses). A stride of the SLIP can be divided into a stance phase, with the foothold fixed on the ground, and a flight phase, where the body follows a ballistic trajectory under the influence of gravity. In the flight phase, the springy leg kinematically obtains its desired position given by the touchdown angle γ^{td}, and in the stance phase, the mass moves forward by compressing and then decompressing the spring. The system is open loop since there is no feedback adjusting the touchdown angle according to the state.

A simulation of the SLIP was constructed in Simulink™. The initial conditions include the forward speed $\dot{x}$ and the vertical height y at apex, while the touchdown angle γ^{td} is kept constant during the periodic motion. In agreement with other results in the literature (cf. Seyfarth et al. 2002; Ghigliazza et al. 2003), it was found that there exists a range of parameter values and initial conditions where the SLIP is asymptotically stable within a particular total energy level.

It is known that for a set of initial conditions, there exists a touchdown angle at which the system maintains its initial forward speed. As Raibert (1986) noted, if the fixed point is perturbed by changing the touchdown angle, e.g. by decreasing it (steeper angles), then the system will accelerate in the first cycle. Thus, at the second step the forward speed will be greater than that at the first, and if the touchdown angle is kept constant and equal to the initial one, the system will accelerate in the subsequent steps and finally fail due to toe stubbing (the kinetic energy increases at the expense of the potential energy resulting in lower apex heights). However, when the parameters are within the self-stabilization regime, the system does not fail. This fact is not captured by Raibert's linear steady state argument, based on which one would be unable to predict the self-stabilization behavior of the system.

A question we address next regards the relationship between the forward speed at which the system converges, called the *speed at convergence*, and the touchdown angle. To this end, simulation runs have been performed, in which the initial apex height and initial forward velocity are fixed, thus the total energy is fixed, while the touchdown angle changes in a range where cyclic motion is achieved. For a given energy level, this results in a curve relating the speed at convergence to the touchdown angle. Subsequently, the apex height is kept constant, while the initial forward velocity varies between 5 and 7 m/s. This results in a family of constant energy curves, which are plotted in Figure 5. It is interesting to see in Figure 5 that in the self-stabilizing regime of the SLIP, an increase in the touchdown angle *at constant energy* results in a lower forward speed at convergence. This means that locally, for constant energy levels, higher forward speeds can be accommodated by smaller touchdown angles, which, at first glance, is not in agreement with the *global* behavior that higher speeds require larger (flatter) touchdown angles. This global behavior is also evident in Figure 5, where it can be seen that forward speeds of about 5 m/s require touchdown angles in the range 21°–23.75°, while higher speeds, such as those about 7 m/s, require larger touchdown angles, which lie in the range 25.75°–30°.

The fact that *globally* fixed points at higher speeds require greater (flatter) touchdown angles was reported by Raibert (1986), and it was used to control the forward speed of his robots based on a feedback control law. However, Figure 5 suggests that in the *absence* of control, i.e., when the system is open loop, and for a constant energy level, a reduction in the touchdown angle results in an increase of the speed at convergence.[5] These findings illustrate that direct applica-

5. It must be mentioned here that the behavior shown in Figure 5 refers to the particular values of initial speed, total energy and touchdown angle used in simulations, and may not be the same for all the possible combinations of values of these parameters.

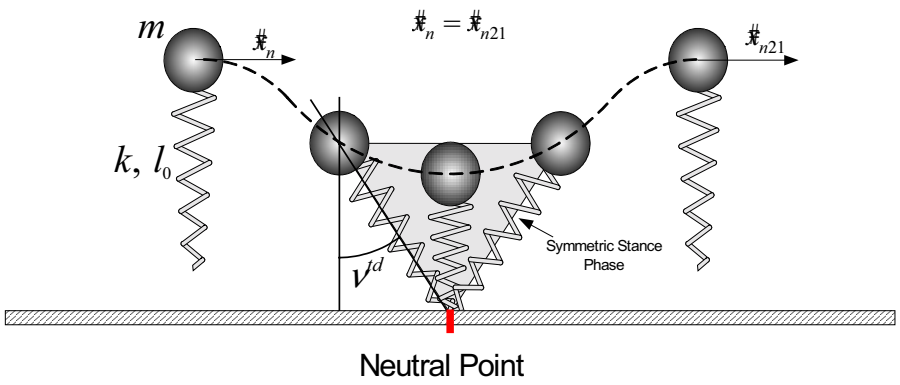

Fig. 4. Spring Loaded Inverted Pendulum (SLIP): neutral point and symmetric stance phase ($m = 80$ kg, $l_0 = 1$ m, $k = 20$ kN / m).

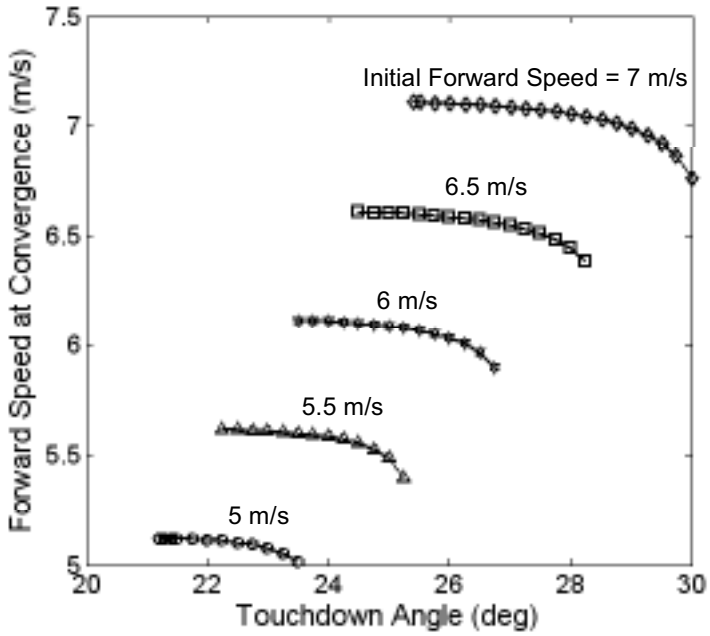

Fig. 5. Forward speed at convergence versus touchdown angle at fixed points obtained for initial forward speeds from 5 to 7 m/s and for an apex height of 1 m.

tion of the above results in intuitive controllers is not trivial (Poulakakis 2002). Note that similar behavior may also hold in quadrupedal models, although the connection with Figure 5 may not be straightforward. These issues, as well as the design of controllers that take into account these properties, are currently under consideration.

Table 1. Basic Mechanical Properties of Scout II

Parameter	Value	Units
Body mass, m	20.865	kg
Body inertia, I	1.3	kg m^2
Spring constant, k	3520	N/m
Hip separation, $2L$	0.552	m
Leg rest length, l_0	0.323	m

4. Modeling the Passive Dynamics of Bounding

Motivated by the stable behavior discovered in the conservative, open loop SLIP, an investigation of the passive dynamics of Scout II in the bounding gait is undertaken in this and the following sections. Despite its utility for describing running in animals and machines of various structures (Full and Koditschek 1999), the SLIP does not capture the body pitch stabilization problem, which is a significant component of the motion in the bounding gait. To overcome this issue, a model for studying the passive dynamics of Scout II in bounding is developed in this section. The goals of the analysis are to determine the conditions required to permit steady state cyclic motion, to understand the fundamentals of the bounding gait followed by the robot, and to find ways to apply these results to improve the performance of dynamically stable robots such as Scout II.

It is well known that legged robots belong in the category of *hybrid* systems and cannot be mathematically described by a single flow. A collection of continuous flows together with discrete transformations governing transitions from one flow to the next are required to model the dynamics of such systems. In this paper we follow the terminology and notation used in Guckenheimer and Johnson (1995). Let J represent a finite index set enumerated by α, and $\hat{X}_\alpha$, $\alpha \in J$, a collection of charts. Here, we are interested in systems that are described by conservative, autonomous, holonomically constrained vector fields $\mathbf{f}_\alpha$ with state variables $\hat{\mathbf{x}} = \begin{bmatrix} \mathbf{q}^T & \dot{\mathbf{q}}^T \end{bmatrix}^T \in \hat{X}_\alpha$ and dynamics $\dot{\hat{\mathbf{x}}} = \mathbf{f}_\alpha(\hat{\mathbf{x}})$. Transitions from vector field $\mathbf{f}_\alpha$ to $\mathbf{f}_\beta$ are governed by discrete equations h_α^β, called threshold functions. Each threshold function specifies an event at its zero crossing. In this paper we are interested in studying the stability of certain orbits, whose appropriate projections are periodic on a recurring sequence of charts, and correspond to the bounding gait.

The model for analyzing the passive dynamics of Scout II in the sagittal plane is presented in Figure 6, while the associated parameters are given in Table 1. Note that this model can also be used to study other sagittal plane running gaits such as pronking, pacing, or trotting, in which the pitch motion is important and cannot be modeled by point mass hoppers like the SLIP.

The index set $J = \{1, 2, 3, 4\}$ includes the four phases that compose the bounding gait described in Figure 3. The indices 1, 2, 3, 4 refer to the flight, the back leg stance, the double leg stance and the front leg stance phase, respectively. The configuration space of each of the phases is parameterized by the Cartesian coordinates $(x, y) \in R^2$ of the torso's COM (center of mass) and the torso's pitch angle $\theta \in S^1$. Thus, all the charts have the same parameterization $\hat{X}_\alpha = R^2 \times S^1 \times R^3 = \hat{X}$, $\alpha \in J$ with state variables $\hat{\mathbf{x}} = \begin{bmatrix} x & y & \theta & \dot{x} & \dot{y} & \dot{\theta} \end{bmatrix}^T$. To derive a simplified mathematical model for Scout II in all the phases, we assume massless legs. Also, a toe in contact with the ground is treated as a frictionless pin joint. In each phase, the equations of motion are obtained using the Lagrangian approach and can be stated in the form

$$\dot{\hat{\mathbf{x}}} = \frac{d}{dt}\begin{bmatrix} \mathbf{q} \\ \dot{\mathbf{q}} \end{bmatrix} = \begin{bmatrix} \dot{\mathbf{q}} \\ -\mathbf{M}(\mathbf{q})^{-1}(\mathbf{F}(\mathbf{q}) + \mathbf{G}(\mathbf{q})) \end{bmatrix} = \mathbf{f}_a(\hat{\mathbf{x}}), \tag{1}$$

where $\mathbf{q} = [\, x \quad y \quad \theta \,]^T$, see Figure 6, and $\alpha \in J$, $\mathbf{M}$ is the mass matrix, and $\mathbf{F}$ and $\mathbf{G}$ are the vectors of the elastic and the gravitational forces, respectively.

As was mentioned in Section 2, we consider two different phase sequences resulting in the two variations of the bounding gait shown in Figure 3. These gaits have been observed in experiments with Scout II. The threshold functions, whose zero crossings determine the touchdown and liftoff events of the front and back virtual legs, are given by the following equations for the bounding with double stance (see Figure 3),

$$h_1^2 = y - L\sin\theta - l_0\cos\gamma_b^{td}, \tag{2a}$$

$$h_2^3 = y + L\sin\theta - l_0\cos\gamma_f^{td}, \tag{2b}$$

$$h_3^4 = l_b - l_0, \tag{2c}$$

$$h_4^1 = l_f - l_0, \tag{2d}$$

and by the following equations for the bounding without double stance (see Figure 3),

$$h_1^2 = y - L\sin\theta - l_0\cos\gamma_b^{td}, \tag{3a}$$

$$h_2^1 = l_b - l_0, \tag{3b}$$

$$h_1^3 = y + L\sin\theta - l_0\cos\gamma_f^{td}, \tag{3c}$$

$$h_3^1 = l_f - l_0, \tag{3d}$$

where the superscript td denotes touchdown, the subscripts b and f denote the back and front virtual legs respectively,

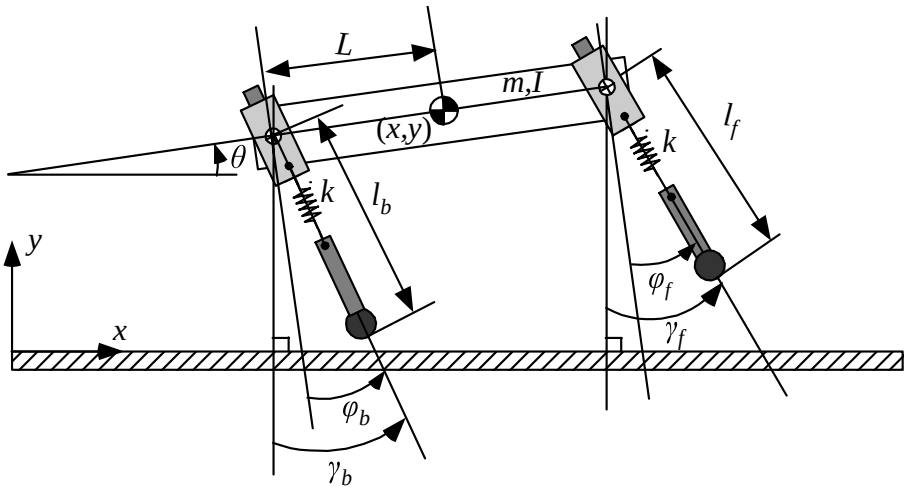

Fig. 6. A template for studying sagittal plane running on Scout II.

and l_0 is the uncompressed leg length, see Table 1. In (2) and (3), zeroing of h_α^β corresponds to the event that signifies the transition from the flow describing phase α to that describing phase β. All the other variables in (2) and (3) are defined in Figure 6. Note that in the second variation of the bounding phase sequence, the dynamics of the double stance phase can be dropped in the calculation of the return map.

To define the return map, we first consider a convenient point in the bounding running cycle. In this work we use the apex height in the double leg flight phase; however, any other point could have been used. We define the Poincaré section (Guckenheimer and Holmes 1983) to be the hyperplane

$$\hat{\Sigma} = \left\{ \hat{\mathbf{x}} \in \hat{X} | \dot{y} = 0,\ y - L\sin\theta > l_0 \cos\gamma_b^{td},\ y + L\sin\theta > l_0 \cos\gamma_f^{td} \right\}, \tag{4}$$

where the conditions $y - L\sin\theta > l_0\cos\gamma_b^{td}$ and $y + L\sin\theta > l_0\cos\gamma_f^{td}$ were added to indicate that the robot is in double leg flight ($\dot{y}$ becomes zero not only at the apex but also at the lowest height). The system is at its apex when its orbit pierces the hyperplane $\hat{\Sigma}$. For the Poincaré map to be properly defined it is necessary that $\hat{\Sigma}$ satisfies the transversality condition (cf. Guckenheimer and Holmes 1983) i.e., the inner product of the vector field and the hyperplane's normal vector must never be zero. In the coordinates $\left(x,\ y,\ \theta,\ \dot{x},\ \dot{y},\ \dot{\theta}\right)$, the normal vector to the hyperplane $\hat{\Sigma}$ is simply $\mathbf{n} = \begin{bmatrix} 0 & 0 & 0 & 0 & 1 & 0 \end{bmatrix}^T$. At apex the vector field is $\mathbf{f}_1\left(\hat{\mathbf{x}}_{\text{apex}}\right) = \begin{bmatrix} \dot{x} & 0 & \dot{\theta} & 0 & -g & 0 \end{bmatrix}^T$, where $\dot{x},\ \dot{\theta} \in R$, since when the system is in the double flight phase it follows a ballistic trajectory. Hence, $\mathbf{n}^T\mathbf{f}_1\left(\hat{\mathbf{x}}_{\text{apex}}\right) = -g \neq 0$, i.e., the transversality condition is satisfied.

We seek a function that maps the apex height states of the n^{th} stride to those of the $(n+1)^{th}$ stride. The states at the n^{th} apex height constitute the initial conditions for the cycle, based on which we integrate the double flight phase equations, until the back leg touchdown event occurs. This event triggers the back leg stance phase, whose dynamic equations are integrated using as initial conditions the final conditions of the previous phase (since massless legs are considered there are no impacts at touchdown). Successive forward integration of the dynamic equations of all the phases, according to (2) and (3) for the two variations of the bounding gait, yields the state vector $\hat{\mathbf{x}}$ at the $(n+1)^{th}$ apex height, which is the value of the Poincaré return map evaluated at the n^{th} apex height. If the state vector at the new apex height is identical to the initial one the cycle is repetitive.

Note though that the state vector contains the horizontal coordinate x of the torso's COM, which is a monotonically increasing function of time. Therefore, x does not map to itself after a cycle, and a function that has been obtained by integrating (1) according to (2) and (3) cannot have fixed points that correspond to the bounding gait. This issue can be resolved by projecting out the horizontal component x of the state vector $\hat{\mathbf{x}}$, which is not relevant to describing the running gait. A further dimensional reduction can be obtained by noticing that on the Poincaré section $\hat{\Sigma}$ the variable $\dot{y}$ is identically zero (this dimensional reduction is inherent to the Poincaré method for stability, see Guckenheimer and Holmes 1983). After the projection $\Pi : \hat{X} \to X; \hat{\mathbf{x}} \mapsto \mathbf{x} = \begin{bmatrix} y & \theta & \dot{x} & \dot{\theta} \end{bmatrix}^T$ of the state vector $\hat{\mathbf{x}} \in \hat{X}$ onto its non x and $\dot{y}$ components, the task of studying passive bounding reduces to finding the fixed points of the return map $\mathbf{P}$ acting on the reduced Poincaré section

with independent coordinates $\mathbf{x} \in X = R \times S^1 \times R^2$, i.e.,

$$\mathbf{x}_{n+1} = \mathbf{P}\left(\mathbf{x}_n, \mathbf{u}_n\right), \tag{5}$$

with $\mathbf{u} = \begin{bmatrix} \gamma_b^{td} & \gamma_f^{td} \end{bmatrix}^T$, and the subscript n indicates the stride number.

Equation (5) represents a nonlinear discrete time system. As expected, despite the fact that the touchdown angles are not part of the state vector and they do not participate in the dynamics, they directly affect the value of the return map. The appearance of the touchdown angles in the right hand side of (5) is a consequence of the dependence of the threshold functions (2) and (3) on the touchdown angles' values. It is apparent from (5) that the touchdown angles are kinematic inputs available for "cheap" control, since, in Scout II, it is very easy to place the legs at their target angles during the flight phase. The significance of the flight phase in the control of running has also been outlined in Altendorfer, Koditschek, and Holmes (2004), where it was shown that, in the passive and conservative SLIP, the stance phase has no contribution to the stability of the gait, while different leg placement strategies during flight result in different stability properties.

5. Existence of Passive Bounding Cycles

5.1. Fixed Points and their Properties

The goal of the analysis in this section is to determine the conditions required to permit steady state cyclic bounding motion of Scout II. In other words we want to find an argument $\mathbf{x}$ in (5) that maps onto itself, i.e., we want to solve the equation

$$\mathbf{x} - \mathbf{P}\left(\mathbf{x}, \mathbf{u}\right) = \mathbf{0}, \tag{6}$$

for all (experimentally) reasonable values of touchdown angles $\mathbf{u}$. Existence of solutions for (6) is not guaranteed, but seems to be the rule rather than the exception.

The search space is 4-dimensional with two free parameters, since for different values of touchdown angles, different solutions may be obtained. The complexity of the equations precludes describing $\mathbf{P}$ as a nonlinear function by analytically integrating the dynamics. Therefore, we resort to numerical evaluation of the return map, and use a Newton-Raphson method for finding its fixed points. Thus, an initial guess $\mathbf{x}_n^{\langle 0 \rangle}$ for the fixed point is assumed and then updated using the equation

$$\mathbf{x}_n^{\langle k+1 \rangle} = \mathbf{x}_n^{\langle k \rangle} + \left(\mathbf{I} - \nabla \mathbf{P}\left(\mathbf{x}_n^{\langle k \rangle}\right)\right)^{-1} \left[\mathbf{P}\left(\mathbf{x}_n^{\langle k \rangle}\right) - \mathbf{x}_n^{\langle k \rangle}\right], \tag{7}$$

where n corresponds to the n^{th} apex height, k corresponds to the number of iterations, and the gradient matrix (Jacobian) of the return map is given by

$$\nabla \mathbf{P} = \frac{\partial \mathbf{P}}{\partial \mathbf{x}} = \begin{bmatrix} \dfrac{\partial \mathbf{P}}{\partial y} & \dfrac{\partial \mathbf{P}}{\partial \theta} & \dfrac{\partial \mathbf{P}}{\partial \dot{x}} & \dfrac{\partial \mathbf{P}}{\partial \dot{\theta}} \end{bmatrix}. \tag{8}$$

To find a solution, we evaluate (7) iteratively until convergence (the error $\left\| \mathbf{x}_n^{\langle k+1 \rangle} - \mathbf{x}_n^{\langle k \rangle} \right\|_\infty < 10^{-5}$). The value of $\mathbf{P}$ at $\mathbf{x}_n^{\langle k \rangle}$ is calculated through the numerical integration of the dynamic equations during a complete cycle. To do that, the adaptive step Dormand-Price method was used in MATLAB™ with $1e-10$ and $1e-9$ relative and absolute tolerances, respectively. To evaluate numerically the Jacobian of the return map, the related partial derivatives are approximated using central differences. Each iteration involves nine evaluations of the return map $\mathbf{P}$: one corresponds to calculating $\mathbf{P}$ at the nominal point $\mathbf{x}_n^{\langle k \rangle}$, and eight to calculate the gradients. More specifically to compute the components $\partial \mathbf{P} / \partial x_i$, $i = 1, \ldots, 4$, of the gradient matrix $\nabla \mathbf{P}$, we need four evaluations of $\mathbf{P}$ at $\mathbf{x}_n^{\langle k \rangle} - d\mathbf{x}$ (fore of the nominal point), and four at $\mathbf{x}_n^{\langle k \rangle} + d\mathbf{x}$ (aft of the nominal point), where $d\mathbf{x}$ is obtained by perturbing each of the components of $\mathbf{x}$ by some small scalar quantity ε (in implementing this scheme we used $\varepsilon = 1e-6$). Evaluating (7) is computationally intensive; however, if the initial guess is reasonable[6] and a solution exists, this method usually finds it in less than eleven iterations.

Using the above method, a large number of fixed points of the return map $\mathbf{P}$ was found, for different initial guesses and different touchdown angles. All these fixed points exhibited some very useful properties concerning the symmetry of the bounding motion. Figure 7 illustrates the evolution of the states during one cycle of the bounding with double stance corresponding to a sample fixed point obtained for touchdown angles $\left(\gamma_b^{td}, \gamma_f^{td}\right) = (16 \text{ deg}, 14 \text{ deg})$, with initial guess $\left(y, \theta, \dot{x}, \dot{\theta}\right) = (0.33 \text{ m}, 0 \text{ deg}, 1.3 \text{m/s}, 120 \text{ deg/s})$. The corresponding fixed point, found after three iterations, is $\left(y, \theta, \dot{x}, \dot{\theta}\right) = (0.324 \text{ m}, 0 \text{ deg}, 1.39 \text{ m/s}, 145.9 \text{ deg/s})$.

It can be seen from Figure 7 that the passively generated bounding motion exhibits symmetric properties about the middle of the double stance phase. Furthermore, as shown in Figure 7, the pitch angle, θ, is zero at the apex height. These characteristics were present in all the fixed points found using the method described above and a large number of initial guesses. Figure 8 illustrates projections of closed bounding orbits of the fixed point presented in Figure 7 on the tangent space showing periodicity. Although Figures 7 and 8 correspond to bounding with double stance phase, the same properties have been observed for the bounding without double stance phase, with the difference that the double stance phase separating the back and front stance phases is replaced by a double flight phase. The corresponding plots for the bounding without double stance phase are not presented here because of space limitations.

Figure 9 presents the leg lengths and the leg angles for the back and front virtual legs during one cycle and for the fixed point of Figure 7. Careful inspection of Figure 9 reveals another important property of the fixed points. It can be seen that

6. Experimentally measured values of the states have been used as initial guesses for finding a fixed point of the return map.

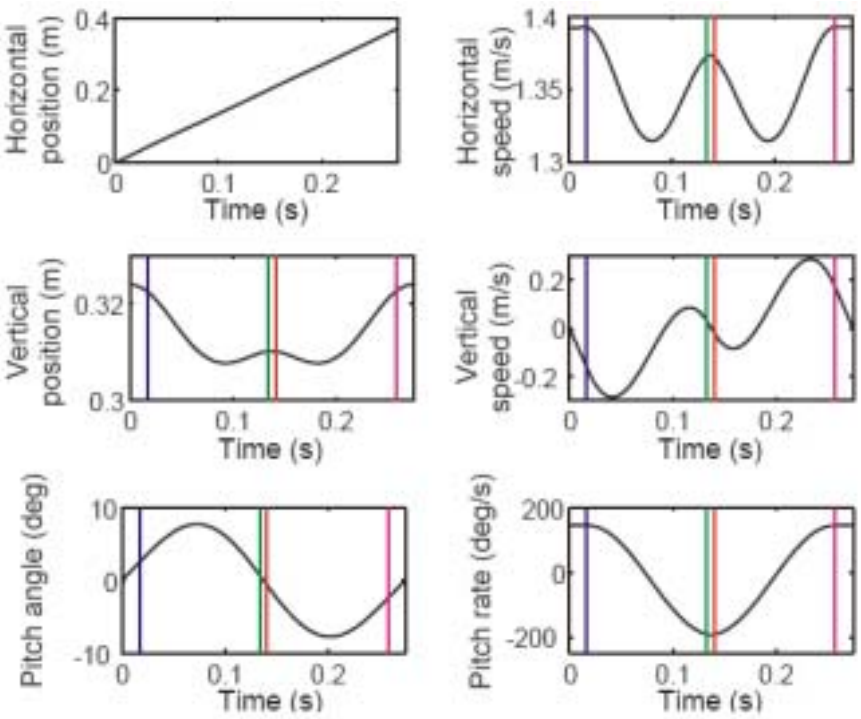

Fig. 7. Evolution of the states at bounding with double stance during one cycle. The vertical lines show the events: back leg touchdown, front leg touchdown, back leg liftoff, and front leg liftoff.

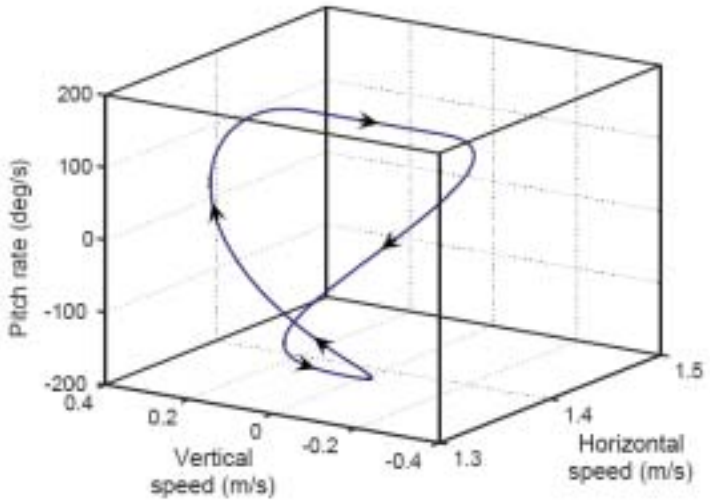

Fig. 8. Projections of bounding orbits on the tangent space for the fixed point shown in Figure 7 (bounding with double leg stance).

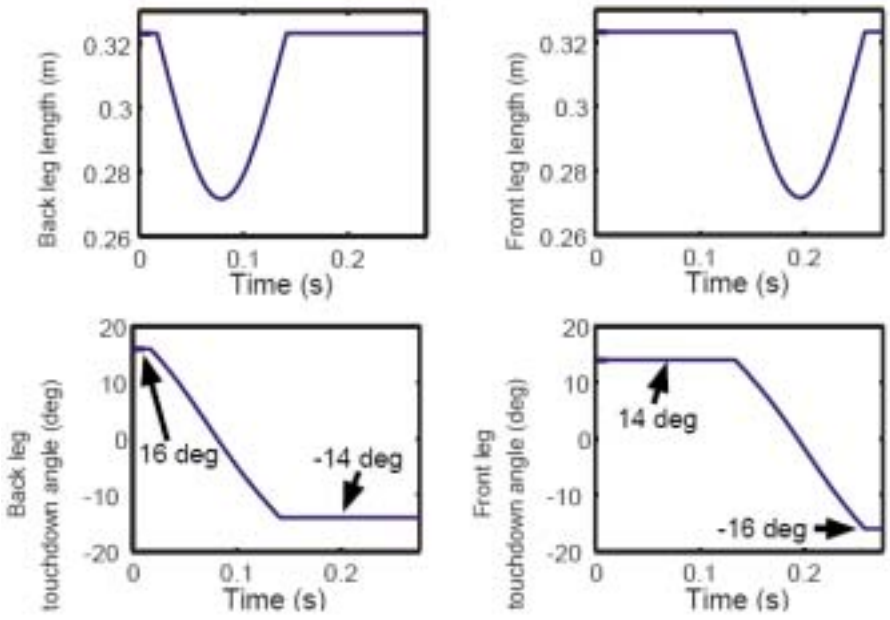

Fig. 9. Evolution of the leg length and angle during a bounding cycle with double stance.

the touchdown angle of the front leg is equal to the negative of the liftoff angle of the back leg, while the touchdown angle of the back leg is equal to the negative of the liftoff angle of the front leg, i.e.,

$$\gamma_f^{td} = -\gamma_b^{lo}, \quad \gamma_b^{td} = -\gamma_f^{lo}, \tag{9}$$

where td and lo denote touchdown and liftoff, while b and f correspond to the back and front legs respectively. The same property has been observed for the bounding without double stance phase. It is interesting to note here that a property similar to (9) was found to hold in the SLIP model, where a necessary and sufficient[7] condition for the existence of fixed points is the stance phase be symmetric, i.e., the liftoff angle is equal to the negative of the touchdown angle (Schwind 1998). Note also, that the notion of symmetric stance phase has been used by Raibert (1986) to maintain or change the forward speed of his robots.

It must be emphasized that in all the results presented in this section the touchdown angles were parameters, which were kept constant. In Section 5.2, the search scheme will be modified using (9), so that the apex height and forward speed—instead of the touchdown angles—are constant parameters for the search. This modification allows for a more systematic way of calculating fixed points of the return map at specific forward speeds and apex heights.

7. This statement was proved for the SLIP assuming that the gravitational force is very small compared to the spring force (Schwind 1998).

5.2. Continuums of Symmetric Fixed Points

For Scout II's bounding running, a specific horizontal speed and a sufficient apex height that prevents toe stubbing are useful functional requirements. Therefore, the search scheme described above is modified in this section, so that the forward speed and apex height become its input parameters, specified according to running requirements and kept constant during the search. The touchdown angles are now considered to be "states" of the searching procedure, i.e., variables to be determined from it. By doing so, the *search space* states and the vector of the parameters ("inputs" to the search scheme) are respectively

$$\mathbf{x}^* = \begin{bmatrix} \theta & \dot{\theta} & \gamma_b^{td} & \gamma_f^{td} \end{bmatrix}^T, \quad \mathbf{u}^* = \begin{bmatrix} y & \dot{x} \end{bmatrix}^T, \tag{10}$$

and the return map whose fixed points are to be calculated becomes

$$\mathbf{x}_{n+1}^* = \mathbf{P}^* \left(\mathbf{x}_n^*, \mathbf{u}_n^* \right). \tag{11}$$

It is important to mention that the numerical integration of the equations of motion starting from the apex height event, results in the calculation of the liftoff angles $\left(\gamma_b^{lo}\right)_n$, $\left(\gamma_f^{lo}\right)_n$ and *not* of the touchdown angles of the legs at the next apex height event. This is a consequence of the assumption of massless legs. Thus, to calculate the gradients needed to implement the Newton-Raphson scheme, the liftoff angles must be "mapped" to touchdown angles based on the symmetry described by (9), i.e.,

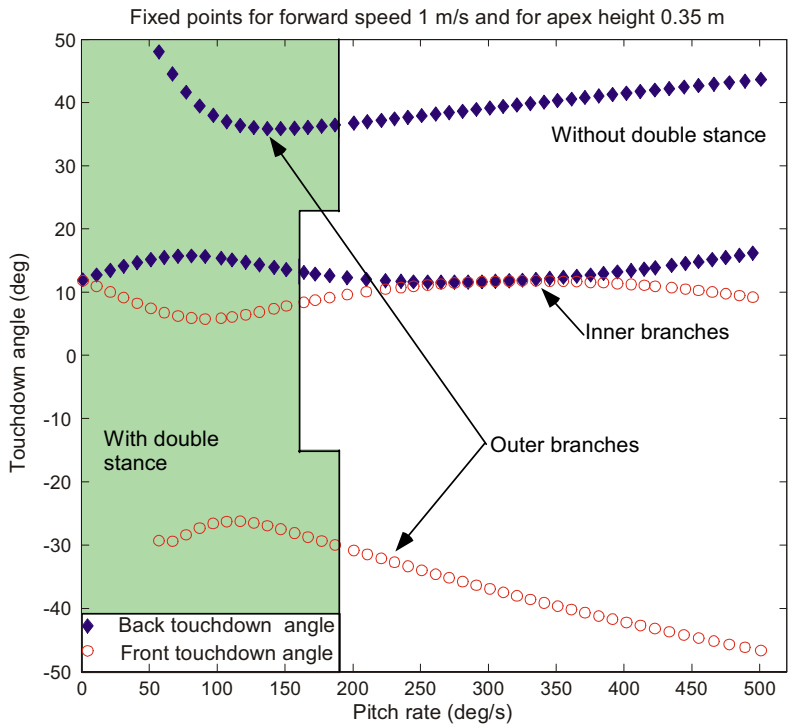

Fig. 10. Touchdown angles versus pitch rates at fixed points for 1 m/s forward speed and 0.35 m apex height. The shadow region corresponds to bounding with double stance phase.

$$\left(\gamma_b^{td}\right)_{n+1} = \left(-\gamma_f^{lo}\right)_n \text{ and } \left(\gamma_f^{td}\right)_{n+1} = \left(-\gamma_b^{lo}\right)_n . \qquad (12)$$

Then, by using the Newton-Raphson algorithm, we update the initial guess until convergence is achieved.

The above search scheme does not explicitly ensure that the following conditions are satisfied,

$$y_{n+1} = y_n, \quad \dot{x}_{n+1} = \dot{x}_n, \qquad (13)$$

which are a direct consequence of the definition of a fixed point. Instead, in the new search scheme, we required that (12) holds. However, examination of the search results shows that, provided that (12) holds, (13) also holds. Note that this behavior is analogous to that of the SLIP, where the symmetric stance phase is a condition for a fixed point (Schwind 1998).

Figure 10 displays the back and front leg touchdown angles at fixed points calculated for 1 m/s forward speed, 0.35 m apex height and varying pitch rate. It can be seen from Figure 10, that there exists a continuum of fixed points, which lie on two inner branches, accompanied by two outer branches. Fixed points lying in the shadow area correspond to the bounding gait with a double stance phase, while fixed points outside this area correspond to the bounding without a double stance phase (cf. Figure 3). It is interesting to note that for both the inner and outer branches, and for some given forward speed and apex height, the system shows preference towards the bounding with double stance for low pitch rates. As the pitch rate, and thus the energy content of the system, increases, the duration of the double stance phase continuously decreases, until a point where it becomes zero. This point signifies the transition from the bounding with a double stance phase to the bounding without; no overlapping between the two variations of the bounding gait is present. It is important to mention that the same tendency has also been observed experimentally with Scout II. For lower system energies the robot converges to a bounding motion with a double stance phase. This fact indicates a qualitative agreement between experiments and the results of Figure 10.

Furthermore, the existence of the outer branches in Figure 10 shows that there is a range of pitch rates where two *different* fixed points exist for the same forward speed, apex height and pitch rate. This is quite surprising, since the same total energy and the same distribution of that energy among the three modes of the motion—forward, vertical and pitch—results in two different motions depending on the touchdown angles. As can be seen from Figure 11, the fixed points that lie on the inner branch correspond to a bounding motion similar to the one observed in experiments with Scout II: the front leg is brought in front of the torso. However, the fixed points that

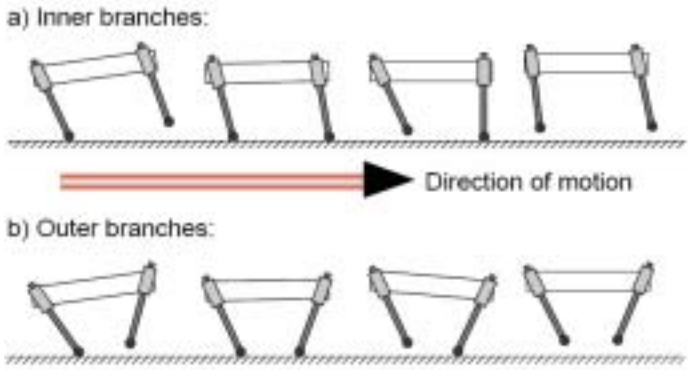

Fig. 11. Snapshots of bounding with double stance motions for the inner and outer branches of Figure 10.

lie on the outer branch correspond to a motion where the front leg is brought towards the torso's COM. The pattern of Figure 11(b) resembles the dynamic walking gait implemented on Scout II, see de Lasa and Buehler (2001), which is only present at lower speeds.

In reading Figure 10, it is useful to note that the region close to the vertical axis corresponds to pronking-like motions. Indeed, recall that at the apex height the pitch angle is always zero ($\theta = 0$; see Figure 7 in Section 5.1). As we approach the vertical axis of Figure 10 ($\dot{\theta} = 0$), the touchdown angles of the front and back legs tend to become equal. A gait with $\theta = 0$, $\dot{\theta} = 0$ and equal touchdown angles for the front and back legs corresponds to the pronking gait, where the front and back legs strike and leave the ground in unison. Therefore, points near the vertical axis correspond to pronking-like motions. This observation will lead to some useful conclusions regarding the stability of the bounding and the pronking gaits, which will be discussed in the next section.

Figure 12 presents fixed points for forward speeds varying from 1 to 4 m/s and for a 0.35 m constant apex height. It can be seen that at higher speeds, the inner branches shift to higher values of the touchdown angles, i.e., larger touchdown angles are required to maintain higher steady state speeds, a fact which is in agreement with Raibert's (1986) findings. In Figure 12 the fixed points marked with "stars" correspond to the transition points from bounding with double stance to bounding without. As can be seen, at higher speeds the transition comes at lower pitch rates demonstrating the experimentally observed fact that at higher energies, the area corresponding to the bounding with double stance (shadow area in Figure 10) shrinks.

Of note is the fact that the fixed points shown in Figure 12 for different forward speeds at the apex correspond to different energy ranges, which do not overlap. This is particularly important for designing controllers since it shows that different speeds require different energies. Therefore, convergence to higher steady state forward speeds cannot occur with the same total energy; see Poulakakis (2002) for more details. As a final remark, note that at higher forward speeds, fixed points lying on the outer branches can still be found. However, larger (in magnitude) touchdown angles are required to keep the system running, i.e., the back and front legs must be very close to each other towards the COM (cf. Figure 11(b)), resulting in physically unrealistic motions. For this reason, Figure 12 presents only the inner branches that correspond to physically common gaits.

6. Local Stability of Passive Bounding

The existence of passively generated bounding running cycles is by itself a very important result, since it shows that an activity as complex as bounding running can simply be a natural motion of the system. However, in real situations the robot is continuously perturbed, therefore, if a fixed point were unstable, then the periodic motion would not be sustainable without control effort. In this section we characterize the stability of the fixed points found in Section 5.

To investigate stability, we assume that the apex height states are perturbed from their nominal values ($\bar{\mathbf{x}}$, $\bar{\mathbf{u}}$), by some small amount ($\Delta\mathbf{x}$, $\Delta\mathbf{u}$). The discrete model that relates the deviations from steady state is

$$\Delta\mathbf{x}_{n+1} = \mathbf{A}\Delta\mathbf{x}_n + \mathbf{B}\Delta\mathbf{u}_n, \tag{14}$$

where $\Delta\mathbf{x} = \mathbf{x} - \bar{\mathbf{x}}$, $\Delta\mathbf{u} = \mathbf{u} - \bar{\mathbf{u}}$ and

$$\mathbf{A} = \partial\mathbf{P}(\mathbf{x},\mathbf{u})/\partial\mathbf{x}\Big|_{\substack{\mathbf{x}=\bar{\mathbf{x}}\\ \mathbf{u}=\bar{\mathbf{u}}}}, \quad \mathbf{B} = \partial\mathbf{P}(\mathbf{x},\mathbf{u})/\partial\mathbf{u}\Big|_{\substack{\mathbf{x}=\bar{\mathbf{x}}\\ \mathbf{u}=\bar{\mathbf{u}}}}.$$

For small perturbations, the apex height states at the next stride can be calculated by the linear difference eqs (14). If all the eigenvalues of the system matrix $\mathbf{A}$ have magnitude less than one, then the periodic solution is stable.

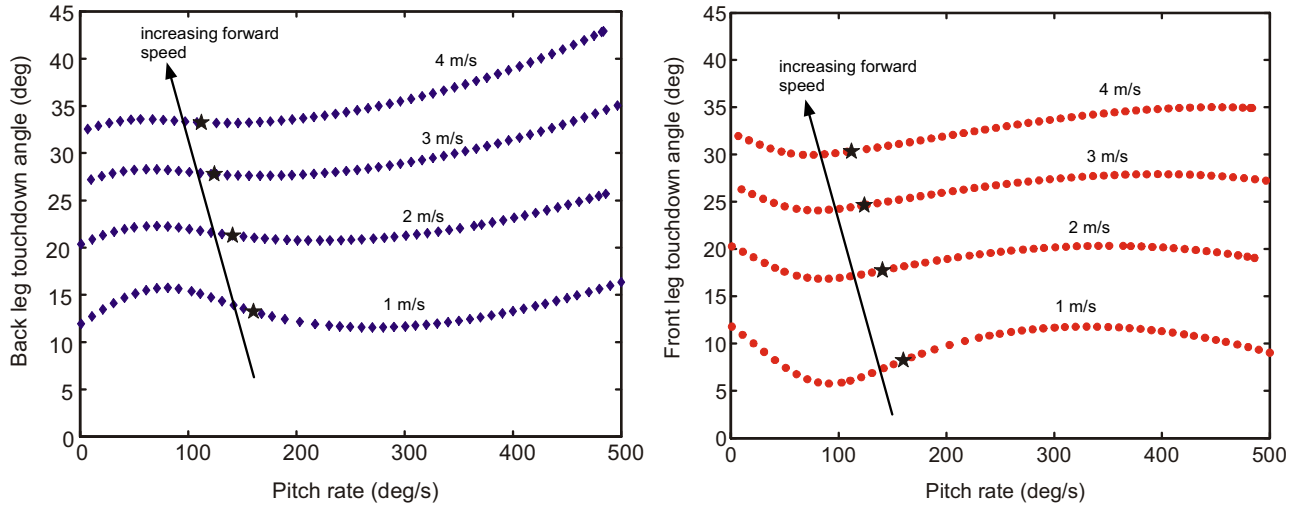

Fig. 12. Fixed points for a 0.35 m apex height and speeds from 1 to 4 m/s. Stars denote transition from bounding with to bounding without double stance phase.

Figure 13 shows the loci of the eigenvalues of matrix **A** for the bounding with and without double stance phase and for both the inner and outer branches of the fixed points presented in Figure 10, as the pitch rate varies. In reading Figure 13 note that the encircled numbers show the initial locations of the eigenvalues, which, as the pitch rate increases, move along the directions of the arrows, on the root locus, and converge to the points marked by "x". As was expected, in all cases, one of the eigenvalues is located at one, representing the fact that the system is conservative[8] (for the sake of clarity the point at which eigenvalue 1 converges is not marked by "x" since it remains always at one). Figure 13(a) corresponds to the inner branch of the bounding with double stance phase (cf. Figure 10). Two of the eigenvalues, namely 2 and 3, start on the real axis, and as $\dot{\theta}$ increases they move towards each other, they meet on the real axis, and finally they move towards the rim of the unit circle. The fourth eigenvalue, marked by 4, starts at a high value and moves towards the unit circle, but it never gets into it, for those specific values of forward speed and apex height. The situation is similar for the outer branch of the bounding with double stance phase, as shown in Figure 13(c). Figures 13(b) and (d) illustrate the loci of the eigenvalues for the inner and outer branches of the bounding without a double stance phase. Again eigenvalue 1 is located at one. Eigenvalues 2 and 3 start at the points where they stopped during the bounding with double stance phase as shown in Figures 13(a) and (c). In Figure 13(b) they move close to the rim of the unit circle, but always stay outside of it. In Figure 13(d) they move in arcs further away from the unit circle until they meet each other on the real axis, after which they move in opposite directions. Eigenvalue 4 starts from the location at which it stopped in the bounding with double stance phase, and in Figure 13(b) it moves on the real axis away from the unit circle, while in Figure 13(d) it moves towards the unit circle.

In all the above cases there is always at least one eigenvalue outside of the unit circle at every value of the pitch rate. Therefore, there is no region of parameters where the system is passively stable for forward speed $\dot{x} = 1$ m / s and apex height $y = 0.35$ m. Note that similar, but not identical, root loci to those presented in Figure 13 are observed at different forward speeds and apex heights, the difference being the values the eigenvalues attain as the pitch rate increases.

To show how the forward speed affects the stability of the motion, we present Figure 14, which shows the magnitude of the larger eigenvalue at different forward speeds for the inner branches of the bounding with and without double stance phase. In this figure, the stars denote transition from bounding with a double stance phase to bounding without one. For sufficiently high forward speeds and for a region of pitch rates, the larger eigenvalue enters the unit circle, while the other two eigenvalues remain well behaved. This fact shows that, for these parameter values, the system is self-stabilized. Furthermore, it is apparent from Figure 14 that the self-stabilization regime is present in both variations of the bounding gait, i.e., with and without double stance phase. It is worth mentioning here that, as depicted in Figure 14, the largest eigenvalue obtains its maximum value when the pitch rate $\dot{\theta}$ is small. Recall that the region where $\dot{\theta}$ takes small values corresponds to a pronking-like motion, where both the front and back legs hit and leave the ground in unison. Thus, we can conclude that

8. The conservative nature of the system could have been used to further reduce the dimension of the Poincaré return map in (5). However, we have decided to keep this extra dimension for reasons of verification.

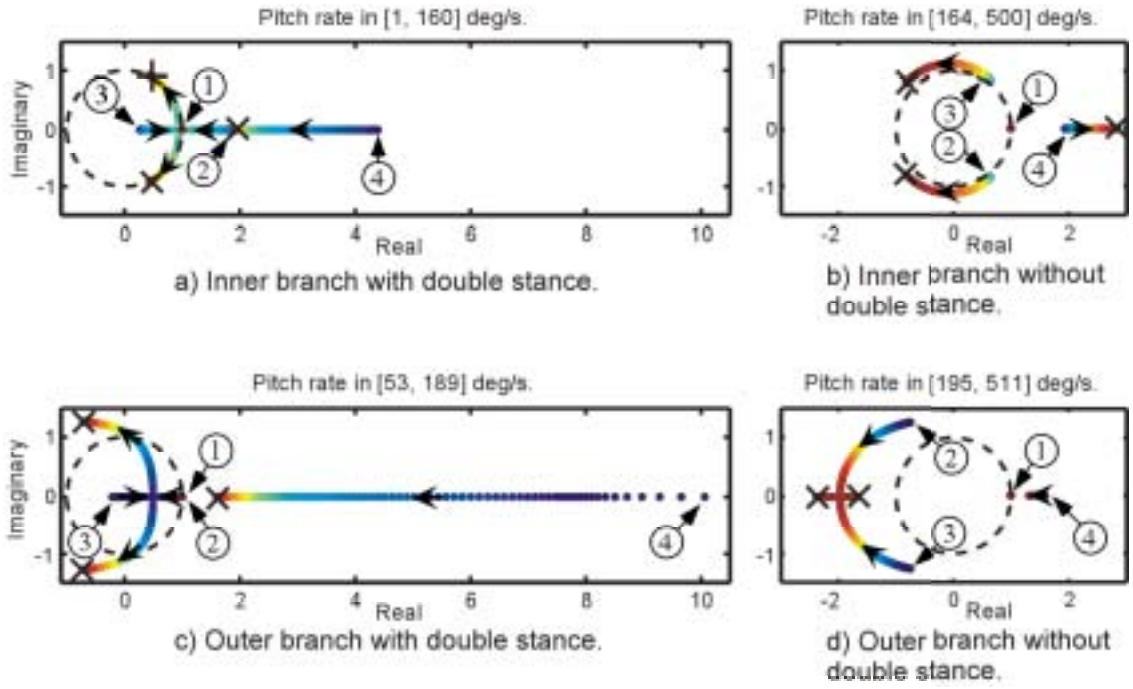

Fig. 13. Root locus showing the paths of the four eigenvalues as the pitch rate increases for the inner (up) and the outer (down) branches of fixed points. The numbers show the starting points of the eigenvalues, "x" denotes the points where the eigenvalues converge, and the arrows show the direction of their motion.

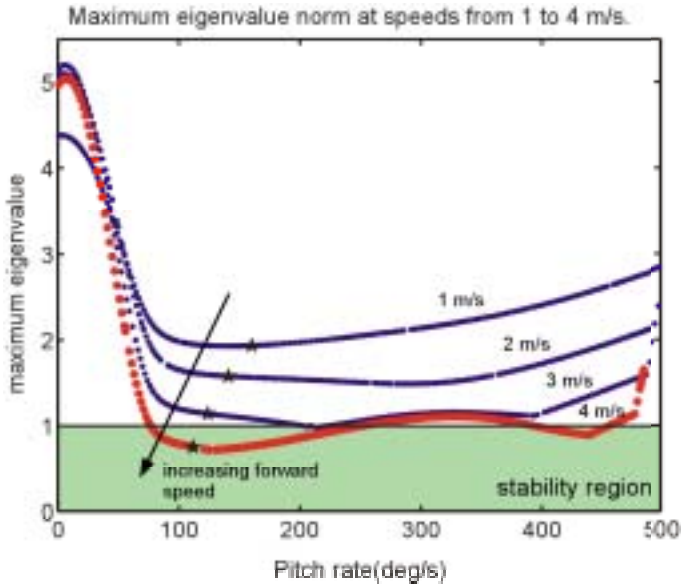

Fig. 14. Largest eigenvalue norm at various pitch rates and for forward speeds 1 to 4 m/s. The stars denote transition from bounding with to bounding without double stance.

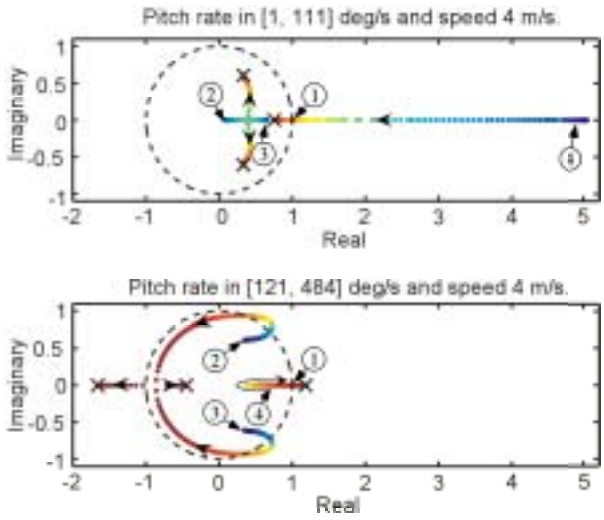

Fig. 15. Root loci for the inner branches of the bounding with (up) and without (down) double stance and for forward speed 4 m/s. The apex height is 0.35 m.

pronking-like motions (low-pitch rates) are "more unstable" than bounding (high pitch rates). This fact was also observed in experiments with Scout II.

The details of the root locus are shown in Figure 15. The shape of the root locus is similar to the root loci presented in Figure 13(a) and (b), except for the fact that, for some values of the pitch rate, eigenvalues 2, 3 and 4 are all inside the unit circle. Note that the changes in the slope of the norm of the larger eigenvalue in Figure 14 are attributed to the fact that, as the eigenvalues move along the branches of the root locus, the eigenvalue that has the larger norm changes; see Figure 15.

Interestingly, despite the apparent simplicity of the quadrupedal model presented above, compared with the complexity of more accurate models of Scout II such as those described in Poulakakis, Smith, and Buehler (2005a), we have been able to reproduce, qualitatively, many different behaviors, which have also been observed experimentally in the robot. These behaviors include both variations of bounding described in Figure 3, and also pronking-like and dynamic walking motions. Furthermore, a good qualitative agreement between the bounding results presented in this paper and the experimental data of Poulakakis, Smith, and Buehler (2005a) has been observed. For instance, the pitch angle as shown in Figure 7 bears remarkable resemblance to the corresponding one measured in experiments (see Figure 12 in Poulakakis, Smith, and Buehler 2005a). Moreover, self-stabilization occurs in a range of pitch rates, which is in agreement with the pitch rates measured in experiments with Scout II. However, experimental Scout II runs are stable at approximately 1/3 the speeds predicted here. This is most probably due to the stance-brake phase present in the controller in experiments; see Figure 2. The stance-brake phase results in decelerating the robot, and breaks the touchdown-liftoff symmetry presented in Figure 9. As is described in detail in Poulakakis, Smith, and Buehler (2005a), it also results in errors between simulation results and experimental data, even in more accurate models of Scout II. However, including the stance-brake phase in the controller is necessary for ensuring toe clearance, especially during the early protraction phase, due to the absence of active control of the leg length during flight.

Furthermore, effects not present in passive models, such as actuator dynamics, damping in the leg prismatic joints, intermittent stick/slip of the foot–ground contact, and energy losses at touchdown due to impact, may contribute to discrepancies between the conservative model studied here and the robot, such as the difference in the forward speed. More specifically, regarding the role of the actuators during stance, it is noted that large peaks in the torques appear at the early phases of the stance-retraction phase. However, as is explained in detail in Poulakakis, Smith, and Buehler (2005a; Figures 14 and 15 therein), motor saturation comes almost immediately after touchdown, resulting in very small torques throughout the stance-retraction phase, until the stance-brake phase is reached. The exact role of the actuator dynamics in the resulting motion is currently under investigation.

The main conclusion from the analysis above is that there exists a regime where the system can be passively stable. This is an important result since it shows that the system can tolerate small perturbations away from the nominal conditions without any control action taken. This fact could provide a possible explanation of why Scout II can bound without the need of complex state feedback, using very simple control

laws that only excite its natural dynamics, and is in agreement with recent research from biomechanics, which shows that, when animals run at high speeds, passive dynamic self-stabilization from a feedforward, tuned mechanical system can reject rapid perturbations and simplify control (Full and Koditschek 1999; Kubow and Full 1999). Analogous behavior has been discovered by McGeer (1989) in his passive bipedal running work, and recently in the SLIP template (Seyfarth et al. 2002; Ghigliazza et al. 2003).

7. Conclusion

In this paper, we studied the dynamics of the bounding running gait of a simple passive and conservative model of our Scout II robot. Based on the analysis of numerically derived return maps, we found that the two variations of the bounding gait, which have been experimentally observed on Scout II, can be passively generated with appropriate initial conditions. Most strikingly, in each bounding variation, there exists a regime where the model stabilizes itself without the need of any control action! This is the first time that more elaborate gaits, such as Scout II's bounding, are found to be inherently stable, and is in agreement with recent results from biomechanics, contributing to the increasing evidence that simple controllers, such as those reported in Poulakakis, Smith, and Buehler (2005a) that operate mostly in the feedforward regime, are adequate in stabilizing a complex dynamic task like quadrupedal bounding. Most importantly, self-stabilization can facilitate the design of more robust, yet minimalistic, controllers for dynamically stable legged locomotion, by deriving control laws that expand the domain of attraction of the self-stable behavior. A simplified model, such as the one presented in this paper, that captures the essentials of the motion, can form the basis of a controlled model in a way similar to that presented in Ahmadi and Buehler (1997, 1999), resulting in high performance combined with great energy efficiency. Proposing such a controller for quadrupeds, and implementing it experimentally on Scout II is our goal. The model presented in this paper provides the first step towards this goal.

Acknowledgments

Support by the Institute of Robotics and Intelligent Systems (IRIS III, a Canadian Federal Network of Centres of Excellence), and by the Natural Sciences and Engineering Research Council of Canada (NSERC) is gratefully acknowledged. The second author would like to acknowledge support by a PENED 2003 Grant by the Hellenic General Research and Technology Secretariat. The work of I. Poulakakis has been supported by an R. Tomlinson Doctoral Fellowship Award and by the Greville Smith McGill Major Scholarship while at McGill University, and by the W. Benton Fellowship at The University of Michigan.

References

Ahmadi, M. and Buehler, M. 1997. Stable Control of a Simulated Running Robot with Hip and Leg Compliance. *IEEE Transactions on Robotics and Automation* 13(1):96–104.

Ahmadi, M. and Buehler, M. 1999. The ARL Monopod II Running Robot: Control and Energetics. *Proceedings of IEEE International Conference on Robotics and Automation*, Detroit, USA, pp. 1689–1694.

Altendorfer, R., Koditschek, D. E., and Holmes, P. 2004. Stability Analysis of Legged Locomotion by Symmetry-Factored Maps. *International Journal of Robotics Research* 23(10–11):979–1000.

Berkemeier, M. D. 1998. Modeling the Dynamics of Quadrupedal Running. *International Journal of Robotics Research* 17(9):971–985.

Berns, K. 2006. Walking Machine Catalogue, http://www.walking-machines.org/ (last accessed March 14, 2006).

Brown, H. B., Jr. 1985. Analysis of Planar Model for Two Limiting Cases. *Technical Report, CMU-LL-4-1985*, Carnegie Mellon University, The Robotics Institute, Pittsburgh, PA, USA.

Buehler, M. 2002. Dynamic Locomotion with One, Four and Six-Legged Robots. *Journal of the Robotics Society of Japan* 20(3):15–20.

Campbell, D. and Buehler, M. 2003. Preliminary Bounding Experiments in a Dynamic Hexapod. *Experimental Robotics VIII*, B. Siciliano and P. Dario (eds), Springer-Verlag, pp. 612–621.

Cham, J. G., Bailey, S. A., and Cutkosky, M. R. 2000. Robust Dynamic Locomotion through Feedforward - Preflex Interaction. *ASME International Mechanical Engineers Congress and Exposition (IMECE)*, Orlando FL.

Cham, J. G., Bailey, S. A., Clark, J. E., Full, R. J., and Cutkosky, M. R. 2002. Fast and Robust: Hexapedal Robots via Shape Deposition Manufacturing. *International Journal of Robotics Research* 21(10):869–882.

Cherouvim, N. and Papadopoulos, E. 2005. Single Actuator Control Analysis of a Planar 3DOF Hopping Robot. *Robotics: Science and Systems I*, S. Thrun, G. Sukhatme and S. Schaal (eds) pp. 145–152, MIT Press, Cambridge MA.

de Lasa, M. and Buehler, M. 2001. Dynamic Compliant Walking. *Proceedings of IEEE International Conference on Robotics and Automation*, Vol. 3. pp. 3153–3158, Seoul, Korea.

Fukuoka, Y., Kimura, H., and Cohen, A. 2003. Adaptive Dynamic Walking of a Quadruped Robot on Irregular Terrain Based on Biological Concepts. *International Journal of Robotics Research* 22(3–4):187–202.

Full, R. J. and Koditschek, D. 1999. Templates and Anchors: Neuromechanical Hypotheses of Legged Locomotion on Land. *Journal of Experimental Biology* 202:3325–3332.

Ghigliazza, R. M., Altendorfer, R., Holmes, P., and

Koditschek, D. E. 2003. A Simply Stabilized Running Model. *SIAM Journal of Applied Dynamical Systems* 2(2):187–218.

Grizzle, J. W., Abba, G., and Plestan, F. 2001. Asymptotically Stable Walking for Biped Robots: Analysis via Systems with Impulse Effects. *IEEE Transactions on Automatic Control*. 46(1):51–64.

Guckenheimer, J. and Holmes, P. 1983. *Nonlinear Oscillations, Dynamical Systems, and Bifurcations of Vector Fields*. Applied Mathematical Sciences, Vol. 42, Springer-Verlag, NY.

Guckenheimer, J. and Johnson, S. 1995. Planar Hybrid Systems. In *Hybrid Systems II, Lecture Notes in Computer Science*, pp. 202–225, Springer-Verlag.

Iida, F. and Pfeifer, R. 2004. Cheap Rapid Locomotion of a Quadruped Robot: Self-Stabilization of Bounding Gait. *Intelligent Autonomous Systems 8*, F. Groen et al. (eds), IOS Press, Amsterdam, The Netherlands, pp. 642–649.

Kimura, H., Akiyama, S., and Sakurama, K. 1998. Realization of Dynamic Walking and Running of the Quadruped Using Neural Oscillator. *Proceedings of the IEEE/RSJ International Conference on Intelligent Robots and Systems*, Victoria, Canada, pp. 406–412.

Kubow, T. and Full, R. 1999. The Role of the Mechanical System in Control: A Hypothesis of Self-stabilization in Hexapedal Runners. *Philosophical Transactions of the Royal Society of London Series B—Biological Sciences* 354(1385):854–862.

McGeer, T. 1989. Passive Bipedal Running. *Technical Report, CSS–IS TR 89-02*, Simon Fraser University, Centre For Systems Science, Burnaby, BC, Canada.

McGeer, T. 1990. Passive Dynamic Walking. *International Journal of Robotics Research* 9(2):62–82.

McMahon, T. 1985. *Muscles, Reflexes, and Locomotion*, Princeton University Press.

Murphy, K. N. 1985. Trotting and Bounding in a Simple Planar Model, *Technical Report, CMU-LL-4-1985*, Carnegie Mellon University, The Robotics Institute, Pittsburgh, PA, USA, February.

Pearson, K. 1976. The Control of Walking. *Scientific American* 72:86.

Poulakakis, I. 2002. *On the Passive Dynamics of Quadrupedal Running*, M. Eng. Thesis, McGill University, Montreal, QC, Canada.

Poulakakis, I., Papadopoulos, E., and Buehler, M. 2003. On the Stable Passive Dynamics of Quadrupedal Running. *Proceedings of the IEEE International Conference on Robotics and Automation*, Taipei, Taiwan, pp. 1368–1373.

Poulakakis, I., Smith, J. A., and Buehler, M. 2005a. Modeling and Experiments of Untethered Quadrupedal Running with a Bounding Gait: The Scout II Robot. *International Journal of Robotics Research* 24(4):239–256.

Poulakakis, I., Smith, J. A., and Buehler, M. 2005b. On the Dynamics of Bounding and Extensions Towards the Half-Bound and the Gallop Gaits. *Adaptive Motion of Animals and Machines*. H. Kimura, K. Tsuchiya, A. Ishiguro, and H. Witte (eds), Springer-Verlag, pp. 79–88.

Raibert, M. H. 1986. *Legged Robots that Balance*. MIT Press, Cambridge MA.

Saranli, U., Buehler, M., and Koditschek, D. E. 2001. RHex: A Simple and Highly Mobile Hexapod Robot. *International Journal of Robotics Research* 20(7):616–631.

Saranli, U. and Koditschek, D. E. 2003. Template Based Control of Hexapedal Running. *Proceedings of the IEEE International Conference on Robotics and Automation*, Taipei, Taiwan, Vol. 1, pp. 1374–1379.

Scheck, F. 1999. *Mechanics: From Newton Laws to Deterministic Chaos*. Third Ed., Springer-Verlag, Berlin.

Schmitt, J. and Holmes, P. 2000. Mechanical models for insect Locomotion: Dynamics and Stability in the Horizontal Plane I. Theory. *Biological Cybernetics* 83:501–515.

Schwind, W. 1998. *Spring Loaded Inverted Pendulum Running: A Plant Model*, PhD Thesis, The University of Michigan, Ann Arbor, MI, USA.

Seyfarth, A., Geyer, H., Guenther, M., and Blickhan, R. 2002. A Movement Criterion for Running. *Journal of Biomechanics* 35:649–655.

Smith, J. A. and Poulakakis, I. 2004. Rotary Gallop in the Untethered Quadrupedal Robot Scout II. *Proceedings of the IEEE/RSJ International Conference on Intelligent Robots and Systems*, Sendai, Japan, pp. 406–412.

Weingarten, J. D., Lopes, G. A. D., Buehler, M., Groff, R. E., and Koditschek, D. E. 2004. Automated Gait Adaptation for Legged Robots. *Proceedings of the IEEE International Conference on Robotics and Automation*, New Orleans, USA, Vol. 3, pp. 2153–2158.

Yamamoto, Y., Fujita, M., De Lasa, M., Talebi, S., Jewell, D., Playter, R., and Raibert, M. 2001. Development of Dynamic Locomotion for the Entertainment Robot—Teaching a New Dog Old Tricks. *4th International Conference on Climbing and Walking Robots*, pp. 695–702.

Zhang, Z. G., Fukuoka, Y., and Kimura, H. 2004. Stable Quadrupedal Running based on a Spring-Loaded Two-Segment Legged Model. *Proceedings of the IEEE International Conference on Robotics and Automation*, New Orleans, USA, Vol. 3, pp. 2601–2606.